Stratigraphy, Paleomagnetism and Cosmogenic-Isotope Burial Dates of Fossil-Bearing Strata within Riverbluff Cave, Greene County, Missouri

Charles W. Rovey II

Department of Geography, Geology, and Planning, Missouri State University
901 S. National, Springfield, MO 65897, USA charlesrovey@missouristate.edu

Greg Balco
Quaternary Research Center and Department of Earth and Space Sciences
University of Washington, Mail Stop 351310, Seattle, WA 98195-1310, USA balcs@u.washington.edu

Present Address:
Berkeley Geochronology Center
2455 Ridge Road, Berkeley, CA 94709, USA balcs@bgc.org

Matt Forir
Missouri Institute of Natural Science
2327 W. Farm Road 190
Springfield, MO 65810
cavehog@hotmail.com

David Gaunt
Missouri Geological Survey
111 Fairgrounds Road, Rolla, MO 65401, USA david.gaunt@dnr.mo.gov

William F. Kean
Department of Geosciences
University of Wisconsin-Milwaukee, P.O Box 413, Milwaukee, WI 53201, USA wkean@csd.uwm.edu

Stratigraphy, Paleomagnetism and Cosmogenic-Isotope Burial Dates of Fossil-Bearing Strata within Riverbluff Cave, Greene County, Missouri

Abstract

Riverblufff Cave is a short single passage between the James River and its direct tributary, Ward Branch. Before stream incision the cave functioned as a spillway/piracy between the two streams during high-discharge events and accumulated a sequence of stratified fluvial sediments throughout the cave. Five cosmogenic-nuclide burial ages for these sediments are in the correct stratigraphic sequence and are consistent with the position of the Matuyama/Brunhes paleomagnetic boundary.

The cosmogenic-nuclide burial dates indicate that sandy channel-facies deposits derived from Ward Branch began to accumulate within the cave as early as 1.08 +/- 0.07 Ma. This coarse-grained sequence is capped by fossiliferous gravel beds dated at 0.74 +/- 0.07 Ma, which contain abundant mammoth bones. By 0.65 +/- 0.08 Ma all Ward-Branch entrances had been abandoned due to incision and a laminated red clay derived from backflow from flooding along the James River capped the older channel sediments.

Introduction

Riverbluff Cave was discovered in late 2001 when a road-construction crew blasted into a highly decorated room near one of the cave's (former) natural entrances (Figure 1). Before the blast all natural entrances had been sealed by various geologic processes; thus, the general condition of the cave prior to closure had been preserved for some unknown duration. Members of the Missouri Speleological Survey (MSS) soon began mapping the cave (Figure 2) and discovered well-preserved trackways and claw marks within and atop an upper sediment layer (Figure 3), along with various rodent, snake, and peccary skeletons. Additionally, fossil remains of larger vertebrates, including horse and mammoth, were visible within a gravel bed within a stratified sequence along the cave's main passage (Table 1, Figure 4). These discoveries prompted Greene County to purchase the land above the cave and establish the Missouri Institute of Natural Science Museum to catalog and preserve the cave's specimens .

Mammoth and horse fossils have previously been found in Missouri and Missouri caves (Hawksley, 1986; Kurtén and Anderson, 1980), but mammoth finds are rare, and these discoveries have rarely, if ever, been made within a precise geologically dateable context. Moreover, peccary trackways apparently have not been found previously in cave sediment (Forir et al., 2007). Therefore, we conducted a series of dating techniques for the strata bearing these fossils to determine or constrain their ages and the general geomorphic and sedimentologic history of the cave.

Setting

Riverbluff Cave is in Greene County, Missouri near the southeast margin of the Springfield Plateau Physiographic Subprovince (Figure 2), which is largely defined by a caprock of the Burlington-Keokuk Formation. This formation is a tightly cemented crinoidal grainstone, which is highly susceptible to karstification and cave development. Over 300 caves have been cataloged for Greene County alone. Most caves of the Springfield Plateau are branchwork or rudimentary/single passage types (Dom and Wicks, 2003), implying origins from point-source recharge within upland sinkholes or swallow holes along sinking streams. Riverbluff Cave (Figure 2) is such a single-passage between Ward Branch and the James River. A short offshoot (East Passage) is sealed from the main passage by breakdown materials and indicates that the cave once may have been part of a more-extensive branchwork system. Current seepage into the cave drains downward from several sump areas, indicating that an undiscovered lower tier may be present and/or developing beneath the explored level.

The top of the Ward-Branch paleoentrance is approximately 13 m above the present channel. After that entrance was abandoned due to incision, it was eventually sealed by a combination of breakdown within the cave and colluvium from the upper bluff. The James-River paleoentrance extends to the top of a terrace approximately 9 m above the modern floodplain. That entrance is choked with fine-grained sediment, possibly a combination of soil colluvium and vertical-accretion (overbank) deposits from the James River.

The Ward-Branch paleoentrance is approximately 3 m higher than the James-River paleoentrance. Thus, the cave floor generally slopes toward the James-River, in accordance with the surface drainage, and sediment normally would have entered the cave from its upstream or Ward-Branch direction. Nevertheless, flooding along the James River could have easily reached the Ward-Branch paleoentrance, flowed back into the cave, and deposited fine-grained suspension sediment.

Cave Development Model

Stock et al. (2005) presented a model, which appears to closely describe the formation, infilling, and abandonment of Riverbluff Cave. Following this model, single-passage caves often develop between a master stream and a swallow hole in a tributary. Coarse sediment is transported from the swallow hole as bed load and deposited within the cave so long as the swallow entrance is very close to the channel elevation. During this time any fine-grained sediment, temporarily deposited during waning flow or as infiltration through the ceiling, is periodically flushed from the cave during high-discharge events. Thus, fine-grained sediment generally does not accumulate during this early phase of sedimentation.

As the tributary incises below the swallow hole, that entrance is abandoned and coarse sediment no longer enters the cave. Thereafter, fine-grained sediment is transported into the cave as suspended load during flooding along the master stream, so long as that entrance is within the maximum flood height. This later sediment caps the earlier coarse materials and becomes finer upward as the main stream incises progressively farther below that entrance. After the backflow ceases and the cave “enters” the vadose zone, speleothems and flowstone eventually form a cap above the detrital sediment.

With minor modifications this model fits the features of Riverbluff Cave (see following section). One potential difference relates to the cave's (inferred) former branchwork pattern. Cave development may have proceeded from the Ward Branch swallow hole until that passage intersected and enlarged an existing conduit in the vicinity of East Passage.

Sediment Sequence

Riverbluff Cave is consistent with the model described above in that coarse-grained detrital sediment is generally overlain by laminated silty clay (Table 2, Figure 5). The coarse sediment must have entered the cave from the upstream (Ward Branch) direction, given the slope toward the James-River paleoentrance. We interpret the fine-grained laminated sediments as a slackwater facies (i.e. Bosch and White, 2004; White, 2007), which was deposited within local sumps, or throughout the cave during flooding along the James River. In discussing these strata we follow conventions established by the MSS in numbering consecutive sediment "layers" from the top down, although we discuss them in geologic sequence (oldest to youngest).

The sediment within Riverbluff Cave is unusual for Missouri caves (Reams, 1998) and elsewhere (White, 1988) in that a consistent sedimentary sequence is present throughout much of the cave (Table 2, Figure 5). The earliest fluvial sediments fully exposed (Layers 9 & 10) are thin (~ 10-20 cm) beds of sandy loam with sparse (≤ 2%) gravel. Layer 10 (older) is preserved locally, but most of the overlying layers can be traced more extensively throughout the cave wherever a flowstone caprock has not buried the younger detrital sediment.

Layer 8, the “gray silt” (~ 50-100 cm) is distinct from all other strata within the cave. It is a gray (gleyed) laminated silt containing abundant organic debris as both wood clasts and humus concentrated within organic-rich laminae. Gleying is locally splotchy and more intense around the organic inclusions, indicating that reduction was at least partly post depositional. Layer 8, while more extensive than Layer 10 below, also appears to be a localized deposit situated above a low area of the cave’s rock floor. We interpret this layer as a deposit from locally ponded water which collected within a slowly draining sump between high-discharge events.

Layer 8 is overlain by coarse gravelly-pebbly sands of variable thickness and with larger boulder clasts, designated as Layers 6 and 7 (the “gravel beds”). The particle-size distribution of these beds is distinctly bimodal; although they contain > 20% clay, the percentage of total fines decreases downward, and fine silt is absent at the base. A current which could prevent deposition of fine silt should have also prevented clay deposition, so the fines likely infiltrated into the gravel from above during deposition of the overlying red clay (see below).

Layers 6 and & 7 are designated as two units, because they are locally separated by a reactivation surface and/or fine-grained laminae, although they are otherwise visually indistinguishable. Both layers have vague foresets and the upper gravel surface is locally hummocky; thus, we interpret the gravel as amalgamated sets of gravel bars, i.e. a channel facies. The gravel contains unusually high concentrations of vertebrate fragments; limited excavation(~ 1 m^3) has yielded over a dozen specimens of six different taxa (Table 1). The high concentration of mammoth bones in particular, and their slightly abraded condition in some cases, raises speculation that these individuals died in the cave and that their skeletons were then reworked by channel flow within the cave.

A fining-upward sequence of laminated red clay (Layers 1-5) rests upon the gravel beds. We interpret the "red-clay" sequence as a slackwater facies ponded by backflow from the James River during floods. Although bedding-plane breaks are present locally within this sequence, they are not generally traceable beyond a few meters. The different "layers" denote uniform (30.5 cm) divisions established by the MSS for surveying and sampling. The upper part of the red clay (Layers 1 & 2) is bioturbated and includes abundant (up to 8% by weight) small fragments of rodent bone. It is unclear whether these bone fragments are detrital, intrusive, or both.

Sometime after deposition, the detrital sedimentary sequence was partially exposed along a small gully in portions of the cave (Figure 5). The red clay (Layers 1-5) is locally capped by speleothems and flowstone, although in several locations stalagmites are partially buried within the clay, indicating contemporaneous detrital and chemical sedimentation.

Dating Methods

Biostratigraphic, Radiocarbon, and U-Th

The major focus of this work is dating the various vertebrate fossils which have been found within Riverbluff Cave. In this section we first summarize some general and preliminary results from more-routine methods, viz. radiocarbon and U-Th. These methods have not provided spectacular results, but have given some age constraints. We then discuss more thoroughly paleomagnetic and cosmogenic isotope techniques, which have provided a detailed chronology for portions of the Riverbluff Cave sediment sequence.

Mammoth (*Mamuthus*) remains in North America imply an approximate age between 1.5 Ma and 10 ka (Kurtén and Anderson, 1980; Graham, 1998, Lister and Bahn, 2007), but beyond this very broad range we had no initial age constraints for the sediment layers and their fossil remains. We first attempted radiocarbon analysis on a peccary tooth recovered from atop the red clay (Layer 1). The result is an open date > ~ 55,000 ^{14}C yrs. B.P. This result, combined with the presence of mammoth remains in layers 6 & 7, provides a very wide, but nevertheless useful, age bracket of ~ 55,000 ka - 1.5 Ma for Layers 1-7.

We attempted to obtain additional age control with U-Th dating (e.g. Dorale et al., 2004) of speleothems. Two stalagmites from atop the red clay (Layer 1) were thus collected, but results to date have been problematic due to low uranium values (Jeff Dorale, University of Iowa, personal communication, 2007). Nevertheless, a few age determinations from one stalagmite have been completed; the oldest so far is approximately 35 ka. This age is consistent with the open radiocarbon date (> ~55,000 ^{14}C yrs. B.P.), but unfortunately provides no additional information. Future U-Th measurements hopefully will provide more precise age constraints on the deposition of the upper red clay.

Paleomagnetics

Measurement of paleomagnetic remanence can provide useful information on cave-sediment age, particularly if used with other techniques (e.g. White, 2007). Paleomagnetic datums within a series of tiered cave passages were first used to estimate stream incision rates in the

Mammoth Cave and Appalachian Plateau regions (Schmidt, 1982; Sasowsky et al., 1995; Springer et al., 1997). More recently, paleomagnetic measurements have been used to compliment and check the consistency and accuracy of cosmogenic-isotope dates of sediment in other caves (Stock et al., 2005).

The possible age range of ~55 ka to 1.5 Ma for sediment layers 1-7 spans portions of two polarity chrons, the Brunhes Normal (0.78 Ma to present) and the Matuyama Reversed (2.6 Ma – 0.78 Ma). Additionally, a short normal subchron (the Jarimillo) occurred between ~1.07 and 0.99 Ma (Cande and Kent, 1995). Therefore, any reversed remanence within these strata would prove a depositional age > 0.78 Ma. A normal detrital remanent magnetization (DRM- the remanence acquired during deposition) would give a presumptive age of < 0.78 Ma, with only a slight chance of an older age coinciding with the Jarimillo Subchron.

We collected 30 samples for paleomagnetic analysis from the fine-grained sediment layers within Riverbluff Cave. Initially we collected four sets of six samples from Layers 8 and 3-5. We avoided sampling coarse-grained sediment, as well as the upper bioturbated portions of the red clay (Layers 1 &2). Five of the six samples in these initial sets were collected for alternating-field (A.F.) demagnetization by pressing an oriented plastic box into a leveled surface within each sampling horizon. A sixth sample per set was collected for thermal demagnetization by casting a plaster cube around a pedestal cut into a leveled surface. After demagnetization of these original 24 samples, we collected six additional samples for thermal demagnetization from Layer 8, for reasons discussed below.

All paleomagnetic samples were subjected to stepwise demagnetization using either A.F. or thermal techniques. After each demagnetization step the sample's magnetic remanence was measured in multiple orientations to help assess the stability of remanence and to determine an optimum demagnetization level. After demagnetization the high and low-frequency magnetic susceptibility was measured for each sample to determine the bulk magnetite content, and its frequency dependence, which is a function of grain size and remanence stability. Later, remanence intensities were measured under a series of applied D.C. fields to construct isothermal remanence curves for one sample per set. The general shape of the IRM curves is particularly diagnostic in distinguishing hematite versus magnetite dominance as the mineral carrier of the magnetic remanence.

Cosmogenic-Isotope Burial Dating

The cosmogenic isotopes ^{26}Al and ^{10}Be are ideally suited for determining depositional ages of quartz-bearing sediment in caves. The general method, termed "burial dating," has been widely used to date cave sediment within tiered passages of cave systems along major drainages and hence to quantify rates of stream incision and landscape development (Granger et al., 1997, 2001; Stock et al., 2004, 2005, 2006; Anthony and Granger, 2004).

The basic idea of burial dating is that cosmic radiation produces these isotopes within quartz grains at a fixed ratio so long as the quartz is at or near the ground surface. If the quartz is then deposited in an environment, e.g. a cave, where it is shielded from cosmic radiation, production stops (or nearly so), the accumulated isotopes decay at different rates, and their ratio changes in proportion to burial time.

In calculating the burial age of Riverbluff-Cave sediments we assume that the quartz grains experienced a two-stage exposure history in which they originated from steady erosion of the watershed upstream of the cave, and were then washed into the cave and have remained buried at their present depth since that time. In contrast to some previous studies, the burial depth of our samples (~26m) was too shallow to completely ignore post-depositional production of nuclides. Given these assumptions and constraints, the ^{26}Al and ^{10}Be concentrations are:

$$N_{10,m} = \frac{P_{10}(0)}{\lambda_{10} + \frac{\varepsilon}{\Lambda}} e^{-\lambda_{10} t_b} + \frac{P_{10}(z_b)}{\lambda_{10}} \left[1 - e^{-\lambda_{10} t_b}\right] \qquad (1)$$

$$N_{26,m} = \frac{P_{26}(0)}{\lambda_{26} + \frac{\varepsilon}{\Lambda}} e^{-\lambda_{26} t_b} + \frac{P_{26}(z_b)}{\lambda_{26}} \left[1 - e^{-\lambda_{126} t_b}\right] \qquad (2)$$

where $N_{i,m}$ is the measured concentration of nuclide *i* at the present time (atoms g^{-1}), $P_i(0)$ is the surface production rate of nuclide *i* (atoms g^{-1} yr^{-1}), λ_i is the decay constant for nuclide *i*, z_b is the burial depth of the sample (g cm^{-2}), $P_i(z_b)$ is the production rate (atoms g^{-1} yr^{-1}) at the burial depth of the sample, ε is the surface erosion rate prior to burial (g cm^{-1} yr^{-1}), t_b is the duration of burial (yr), and Λ is the effective attenuation length for spallogenic production (here taken to be 160 g cm^{-2}). The first term on the right-hand side of these equations is the formula for the nuclide concentration in a steadily eroding surface, with a radioactive decay factor applied to correct it to the present time; the second term is the nuclide inventory produced at the sample depth during the period of burial. If the sample is deeply buried, the second term is much smaller than the first term. Given the sample depth, the measured ^{26}Al and ^{10}Be concentrations, a knowledge of the nuclide production-depth function $P(z)$, and the decay constants, this pair of equations can be solved to yield the surface erosion rate and the burial age. Granger (2006) gives further details, as well as a complete summary of the development and applications of burial dating. We provide additional discussion specific to Riverbluff Cave in the supplimentary materials (Appendix I).

Several geologic processes could potentially violate our assumption of a two-stage burial history for these samples, and thus introduce systematic errors into the burial ages. First, if the samples experienced a long period of burial elsewhere before being deposited in the cave, their ^{26}Al and ^{10}Be concentrations would not be in equilibrium with steady surface erosion. In effect they would have a burial age greater than zero at the time they were buried at their present site. However, the geomorphic context of this site makes this possibility very unlikely; both Ward Branch and the James River are relatively small catchments that lack thick terraces or floodplain deposits in which sediment could be sequestered for a significant time before deposition in the cave. For example, the alluvium along Ward Branch is generally less than one meter thick. Cutbank exposures of the current James-River floodplain upstream from Riverbluff Cave are also thin, typically <2 m. Thus, there is little possibility of significant burial of the sediment before deposition within the cave.

Second, if sediment within the cave were eroded and redeposited, its burial age would reflect the time of initial entry into the cave rather than emplacement at its present location. Stock et al. (2005), for example, invoked this possibility to account for discrepancies between burial ages and magnetic polarity in Sierra Nevada caves. However, the stratigraphy at Riverblurff Cave again renders this possibiility unlikely because the sediment package is upward-fining, reflecting the transition from active stream-bed deposition to slackwater (suspension) deposition. Later flows into the cave were apparently not competant to remobilize sand-size grains used in the analysis. Additionally, the cave is relatively small and directly fed from river channels. Unlike previous studies, Riverbluff Cave is not an extensive cave system where upstream passages could contribute previously buried sediment to downstream passages. In summary, the geologic and geomorphic conditions of the cave strongly support a simple two-stage exposure history for our samples. In addition, we argue later that the stratigraphic consistency among dates further renders the possibilities of prior burial and redeposition within the cave unlikely.

Our highest priority was to bracket as closely as possible the depositional age of the gravel beds. Many vertebrate fossils are preserved within the gravel, especially along the boundary between Layers 6 & 7, so we first took a composite sample from the middle of the gravel spanning both of these layers. We then sampled above the gravel near the base of the red clay (Layer 5) and directly below the gravel within the top of the gray silt (Layer 8). Later, as excavation progressed, we took two additonal samples in subjacent Layers 9 & 10 as an additional check for stratigraphic consistency in dates. We avoided sampling higher in the red clay due to the low concentration of sand-sized quartz grains.

Results and Interpretations

Paleomagnetics

Paleomagnetic measurements of the red clay (Layers 3-5) are easy to interpret. Results from the gray silt (Layer 8) are complex, but informative. Therefore, we first summarize results from Layers 3-5, and then discuss at greater length measurements from the gray silt.

All samples from the red clay in Layers 3-5 had a stable normal-polarity detrital remanent magnetization (DRM) (Table 3). Mean inclinations are close to the expected dipole value for this latitude (~56°), while declinations are close to due north with a small but consistent westerly deviation. Remanence directions were stable upon step demagnetization with consistent normal orientations. Vector-intensity plots (Figure 6a) of the measured orientations are virtually straight lines trending toward the origin, indicating that a single magnetic remanence is present. These samples had median destructive A.F. fields in the range of 10-15 mT, indicating a remanence carried predominantly by single-domain magnetite grains, which are ideal for retaining a stable DRM. Isothermal Remanent Magnetization (IRM) measurements confirm that magnetite is the principle magnetic mineral, as the samples are essentially saturated by 200-300 mT. Alternating-field demagnetization of these samples was nearly complete by 40-50 mT, implying insignificant amounts of hematite or iron hydroxides which may form authigenically and record a secondary chemical remanent magnetization (CRM). In summary, all paleomagnetic evidence is consistent with deposition of the red clay during a normal-polarity magnetic field. Together with the biostratigraphic constraints, these results indicate that the red clay is almost certainly younger than the most-recent polarity transition at 0.78 Ma.

Results from the gray silt (Layer 8) are not as simple. First, the direction of magnetization is inconsistent, and second, both normal and reversed orientations are present in many samples (Table 4, Figures 6b,c).

Of the initial six samples from Layer 8, the five subjected to A.F. treatment did not demagnetize under peak fields up to 100 mT; this remanence is very hard and therefore cannot be carried by magnetite. Consistent with the hard remanence, which is characteristic of hematite, the intensity of the natural remanent magnetization (NRM) of Layer-8 samples was approximately one tenth to one twentieth that of the samples in the overlying red clay. This difference is also consistent with lower bulk susceptibility values (a proxy measure of magnetite content) in the same ratio. Moreover, IRM curves from these samples do not saturate in fields exceeding 2000 mT, confirming hematite dominance.

The sixth specimen of the initial set from Layer-8 began to demagnetize under thermal treatment, but the plaster containing the sample disintegrated before demagnetization was complete. We therefore took six additional samples from the gray silt at a new location for thermal demagnetization. These samples demagnetized nicely, but again with mixed orientations; nearly all samples revealed reversed components during demagnetization. Most inclinations of the thermally demagnetized samples from Layer-8 are shallow, while declinations, whether normal or reversed, generally have a prominent westerly component.

We speculate that any depositional remanence within the gleyed sediment of Layer 8 was destroyed by post-depositional chemical reduction and concomitant iron-oxide dissolution (e.g. Karlin and Levi, 1985; Canfield and Berner, 1987). Afterward, a weak secondary CRM was acquired as oxidizing conditions were re-established, and authigenic hematite crystallized over an extended time spanning the Matuyama/Brunhes reversal. The dominant polarity measured for any given sample would thus depend on local variation in the rate of crystallization before and after this reversal. The shallow inclinations of most samples are the result of vector averaging of two opposite orientations. Likewise, the declinations' distinct westerly component is the average of a reversed orientation in some grains and a normal orientation in others.

In summary, samples from the gray silt (Layer 8) lack significant amounts of magnetite and a primary or depositional magnetic remanence. They do, however, retain a secondary CRM carried by hematite, which is a complex mixture of both normal and reversed-polarity components. Nevertheless, the common preservation of reversed polarity proves that Layer 8 was subjected to a reversed-polarity field. Therefore, Layer 8 and all subjacent strata must be > 0.78 Ma old.

Burial Dating

The burial ages determined from the cosmogenic-isotope ratios range from approximately 1.08 Ma (Layer 10) to 0.65 Ma (Layer 5) with total uncertainties (1-σ) < 0.10 Ma in all cases (Figure 7, Table 5). A rigorous discussion of methodology and error analysis is given in Appendix I. The ages of adjacent samples (successive layers) generally overlap within 1-σ error limits, but all five ages are consistent with their relative stratigraphic position.

The range in burial dates spans the Matuyama/Brunhes polarity transition, as inferred from paleomagnetic measurements. The oldest date determined so far (1.08 +/- 0.07 Ma, Layer 10) is slightly older than the Jarimillo Normal Polarity Subchron (1.07 – 0.99 Ma). Thus, sediment deposition within Riverbluff Cave may have spanned additional magnetic reversals, although no additional paleomagnetic datums have been found so far due to the lack of fine-grained sediment beneath the gray silt (Layer 8).

Discussion

The burial dates (1.08 – 0.65 Ma, Table 5) are consistent with all paleomagnetic and biostratigraphic constraints discussed above. The magnetic polarity sequence, in particular, provides fairly "tight" control on the burial ages. The burial age near the base of the red clay (Layer 5- normal polarity) is 0.65 +/- 0.08 Ma, slightly younger than the Matuyama/Brunhes transition at 0.78 Ma. The subjacent gray silt (Layer 8 – reversed), approximately 60 cm below the red clay, gives a burial age of 0.90 +/-0.07 Ma, just slightly older than the same paleomagnetic datum. The intervening gravel bed (Layers 6 &7) gives an intermediate burial age of 0.74 +/- 0.07 Ma, which is indistinguishable within error limits from the Matuyama/Brunhes boundary.

In summary to this point, (1) the respective burial ages are in the correct stratigraphic order, and (2) the burial ages are consistent with the Matuyama/Brunhes datum between layers 5 and 8. This consistency strongly suggests that the assumptions involved in the burial dating are valid. If either redeposition or pre-bural of the sediment had introduced any significant systematic error, a correct stratigraphic order and consistency with the magnetic boundary would be very unlikely.

These dates therefore provide firm constraints on the age of the lower sedimentary sequence in Layers 5-10. Sediment began to accumulate within the cave as early as 1.08 +/-0.07 Ma. This phase of sedimentation lasted until 0.74 +/- 0.07 Ma, when the channel-facies sequence was capped by the gravel beds, which contain abundant vertebrate fragments, including horse and mammoth.

The oldest sediments are divided into an upper and lower channel facies by the gray silt (Layer 8), a localized fine-grained layer dated at 0.90 +/- 0.07 Ma. We have interpreted the gray silt as a sump deposit which accumulated between major discharge events. Nevertheless, the gray silt may also be related to deteriorating landscape stability and increased sediment input into the cave. The average surficial erosion rate(~0.002 mm/year) for this sediment (Figure 7, Table 5) is approximately double that for all other layers, and the 0.90 Ma age coincides closely with the onset of the Mid Pleistocene climate transition and the change from 41-ka to 100-ka climate cycles (Ruddiman and Wright, 1987; Raymo et al., 1997; Lisiecke and Raymo, 2005). The longer cycles allowed more extreme climate variability, and geomorphic effects of this transition are widely recorded by massive cave deposits in the Mammoth Cave and Appalachian Plateau regions (White, 2007). Thus, deposition of Layer 8 may relate to climate events which led to cave deposits over large portions of the U.S.

The fossiliferous gravel beds (Layer 8), which cap the channel-facies deposits, extend to the Ward-Branch paleoentrance; thus, that entrance was an active swallow hole at around 0.74 Ma, but was abandoned due to incision thereafter. High-discharge events either transported the vertebrate fragments into the cave from the Ward-Branch drainage basin, or reworked skeletal remains from individuals that died within the cave. The former possibility may imply some sort of mass mortality along the Ward-Branch channel at this time, while the latter would indicate that mammoths and other vertebrates occupied the cave at ~0.74 Ma.

Given that the top of the Ward-Branch paleoentrance is approximately 13 m above the modern channel, the apparent long-term incision rate for Ward Branch is around 0.018 mm/year, approximately 10-20 times greater than the average surface erosion rate (Figure 7) within the drainage basin. This incision rate is based on the elevation at the top of the paleoentrance (the bottom is not exposed), but nevertheless seems incompatible with the possibility that the Ward-Branch paleoentrance remained an active swallow hole during deposition of the entire channel-facies sequence, which spanned some 0.43 Ma. Additional upstream entry points possibly supplied the sediment for lower sandy beds (Layers 9 & 10) through the now-sealed East Passage.

By 0.65 +/- 0.08 Ma (burial age near the base of the red clay) all Ward-Branch entrances were abandoned and backflow from flooding along the James River was the only significant source of detrital sediment for the cave. These backflows deposited a fining-upward sequence of laminated red clay atop the coarse-grained channel facies as the James River incised below the cave’s downstream paleoentrance.

Summary and Conclusions

Burial ages determined for 5 distinct strata within Riverbluff Cave range from 1.08 – 0.65 Ma with total error limits < 0.10 Ma in all cases. The five dates are in the correct stratigraphic order and are consistent with biostratigraphic constraints and the position of the Matuyama/Brunhes paleomagnetic datum within the strata.

The cave sediment generally is a fining-upward sequence reflecting the transition from coarse-grained bedload (upstream, Ward Branch sources) to suspended load (downstream, James River source), as the rivers progressively entrenchment beneath their paleoentrances.

Deposition of channel-facies sediment began by 1.08 +/-0.07 Ma and coarse-grained sediment was deposited intermittently until 0.74 +/- 0.07 Ma. This long duration, which was interrupted by localized accumulations of silty “sump” deposits, likely reflects the contribution of sediment from various swallow holes along Ward Branch. The coarse-grained sediments are capped by highly fossiliferous gravel beds. The reason for the high concentration of vertebrate fossils, notably mammoth and horse, remains speculative, but their age is closely constrained at 0.74 +/- 0.07 Ma, which is within error limits of the Matuyama/Brunhes magnetic boundary.

After deposition of the gravel beds and by 0.65+/- 0.08 Ma, all Ward-Branch entrances had been abandoned and backflows from flooding along the James River were the only sources of detrital sediment. These floods deposited a fining-upward sequence of silt-rich and then clay-rich laminated red sediment. The age of the upper red clay is poorly constrained, because it lacks sand-sized grains which are necessary for the isotopic measurements required for burial dating. Additional U-Th dating of stalagmites partially buried within the upper clay may provide better control on the age of the upper red clay and the age of vertebrate fossils and trackways atop this sediment.

References

Anthony, D.M., and Granger, D.E., 2004, A Late Tertiary origin for multilevel caves along the western escarpment of the Cumberland Plateau, Tennessee and Kentucky, established by cosmogenic ^{26}Al and ^{10}Be: Journal of Cave and Karst Studies, v. 66, no. 2, p. 46-55.

Bosch, R.F., and White, W.B., 2004, Lithofacies and transport of clastic sediments in karstic aquifers, in Sasowsky, I.D. and Mylroie, J., eds., Studies of cave sediments. Physical and chemical records of paleoclimate: New York, Kluwer Academic/Plenum Publishers, p. 1-22.

Cande, S.C. and Kent, D.V., 1995, Revised calibration of the geomagnetic polarity timescale for the Late Cretaceous and Cenozoic: Journal of Geophysical Research, v. 100, no. B4, p. 6,093-6,095.

Canfield, D.E., and Berner, R.A., 1987, Dissolution and pyritization of magnetite in anoxic marine sediments: Geochimica et Cosmochimica Acta, v. 51, p. 645-659.

Dom, J.E., and Wicks, C.M., 2003, Morphology of the Caves of Missouri: Journal of Cave and Karst Studies, v. 65, no. 3, p. 155-159.

Dorale, J.A., Edwards, R.L., Alexander, E.C. Jr., Shen, C., Richards, D.A., and Cheng, H., 2004, Uranium-series dating of speleothems: current techniques, limits, & applications, in Sasowsky, I.D., and Mylroie, J., eds., Studies of cave sediments. Physical and chemical records of paleoclimate: New York, Kluwer Academic/Plenum Publishers, p.177-197.

Forir, M., Ciampaglio, C., and Ryan, N., 2007, Preliminary investigation of the trackways and claw marks within the Riverbluff Cave system: New Mexico Museum of Natural History and Science, Bull. 42, p. 3-4.

Graham, R.W., 1998, The Pleistocene terrestrial mammal fauna of North America, in Janis, C.M., Scott, K.M., and Jacobs, L.K., eds., Evolution of Tertiary Mammals of North America. Volume 1: Terrestrial Carnivores, Ungulates, and Ungulatelike Mammals: Cambridge University Press, p. 66-71.

Granger, D.E., 2006, A review of burial dating methods using ^{26}Al and ^{10}Be, in Siame, L.L., Bourlès, D.L., and Brown, E.T., eds., In situ-produced cosmogenic nuclides and quantification of geological processes: GSA Special Paper 415, p. 1-16

Granger, D.E., Kirchner, J.W., and Finkel, R.C., 1997, Quaternary downcutting rate of the New River, Virginia, measured from differential decay of cosmogenic ^{26}Al and ^{10}Be in cave-deposited alluvium: Geology, v.25, no., 2, p.107-110.

Granger, D.E., Fabel, D., and Palmer, A.N., 2001, Pliocene-Pleistocene incision of the Green River, Kentucky, determined from radioactive decay of cosmogenic ^{26}Al and ^{10}Be in Mamoth Cave sediments: GSA Bulletin, v. 113, no. 7, p. 825-836.

Hawksley, O., 1986, Remains of Quaternary vertebrates from Ozark caves and other miscellaneous sites: Missouri Speleology, v. 26 (1-2), 67 p.

Heisinger, B., Lal, D., Jull, A.J.T, Kubic, P. Ivy-Ochs, S., Neumaier, S., Knie, K.,Lazarev, V., and Nolte, E., 2002a, Production of selected cosmogenic radionuclides by muons: 1. Fast muons: Earth and Planetary Science Letters, v. 200, no. 3-4, p. 345-355.

Heisinger, B., Lal, D., Jull, A.J.T, Kubic, P. Ivy-Ochs, S., Knie, K.,Lazarev, V., and Nolte, E., 2002b, Production of selected cosmogenic radionuclides by muons: 2. Capture of negative muons. Earth and Planetary Science Letters, v. 200, no. 3-4, p. 357-369.

Karlin, R., and Levi, S., 1985, Geochemical and sedimentological control of the magnetic properties of hemipelagic sediments: Journal of Geophysical Research, v. 90, no. B12, p. 10,373-10,392.

Kurtén, B., and Anderson, E., 1980, Pleistocene mammals of North America: New York, Columbia University Press, 442 p.

Lisiecke, L.E., and Raymo, M.E., 2005, A Pliocene-Pleistocene stack of 57 globally distributed benthic $\delta^{18}O$ records: Paleoceanography, v. 20, PA 1003 doi:10.1029/2004PA001071.

Lister, A., and Bahn, P., 2007, Mammoths: Giants of the Ice Age: Berkeley, University of California Press, 192 p.

Nishiizumi,K, Imamura, M., Caffee, M., W., Southon, J., R, Finkel, R., C., and McAnich, J.,A.,2007, Absolute calibration of ^{10}Be AMS standards. Nuclear Instruments and Methods in Physics Research B, v. 258, p. 403-413.

Raymo, M.E., Oppo, D.W., and Curry, W., 1997, The mid-Pleistocene climate transition: A deep sea carbon isotopic perspective: Paleoceanography, v. 12, no. 4, p. 546-559.

Reams, M.W., 1998, Cave sediments and the geomorphic history of the Ozarks: Missouri Speleology, v. 38, no. 1-4, p. 1-97.

Ruddiman, W.F., and Wright, H.E., Jr., 1987, Introduction, in Ruddiman, W.F. and Wright, H.E., Jr. eds., North America and adjacent oceans during the last deglaciation: Boulder Colorado, Geological Society of America, The Geology of North America, v. K-3, p. 1-12.

Sasowsky, I.D., White, W.B., and Schmidt, V.A., 1995, Determination of stream-incision rate in the Appalachian plateaus by using cave-sediment magnetostratigraphy: Geology, v. 23, no. 5, p. 415-418.

Schmidt, V.A., 1982, Magnetostratigraphy of sediments in Mammoth Cave, Kentucky: Science, v. 217, p. 827-829.

Springer, G.S., Kite, J.S., and Schmidt, V.A., 1997, Cave sedimentation, genesis, and erosional history in the Cheat River Canyon, West Virginia: GSA Bulletin, v. 109, no. 5, p. 524-532.

Stock, G.M., Anderson, R.S., and Finkel, R.C., 2004, Pace of landscape evolution in the Sierra Nevada, California, revealed by cosmogenic dating of cave sediments: Geology, v. 32, no. 3, p. 193-196.

Stock, G.M., Granger, D.E., Sasowsky, I.D., Anderson, R.S., and Finkel, R.C., 2005, Comparison of U-Th, paleomagnetism, and cosmogenic burial methods for dating caves: Implications for landscape evolution studies: Earth and Planetary Science Letters, v. 236, p. 388-403.

Stock, G.M., Riihimaki, C.A., and Anderson, R.S., 2006, Age constraints on cave development and landscape evolution in the Bighorn Basin of Wyoming, USA: Journal of Cave and Karst Studies, v. 68, no. 2, p. 76-84.

White, W.B.,1988, Geomorphology and hydrology of karst terrains, New York, Oxford, Oxford University Press, 464 p.

White, W.B., 2007, Cave sediments and paleoclimate: Journal of Cave and Karst Studies, v. 69, no.1, p. 76-93.

Figure Captions

Figure 1. View into Riverbluff Cave from Near the Blast Entrance.

Figure 2. Location and Cave Map.

a. Physiographic Map of Missouri and Green County. Shading shows the general area of the Springfield Plateau; the small box is the approximate location of Riverbluff Cave.

b. Cave Map superimposed on aerial photograph. Dots are survey points, mostly within cave. Cox Road is oriented approximately north-south; the field of view is approximately 800m x 1000m. The main passage of Riverbluff Cave is approximately 760m between the paleoentrances. The cave map is a scanned image of the original hand-drawn map completed by the Missouri Speleological Society (MSS), James Corsentino, cartographer.

Figure 3. Peccary Tracks in Upper Layer of Cave Sediment. The tracks match the size and form of a peccary foot found in the same passage. Photo was taken near the junction with East Passage (Figure 2b). Prints are approximately 8 cm long.

Figure 4. Mammal Fossils within the gravel beds in Riverbluff Cave.

a. Mammoth tibia. Ruler is 15 cm long.

b. Horse metacarpal.

Figure 5. Sedimentary Strata within Riverbluff Cave. See Figure 2b for approximate location. Photograph shows Layers 4-9. Layers 6/7 are the fossiliferous gravel beds. Yellow pins are survey markers approximately 60 cm apart; excavations are sample sites for both paleomagnetic and cosmogenic-isotope analyses.

Figure 6. Vector-Intensity Plots Illustrating Demagnetization of Riverbluff Cave Sediment. Units are those of magnetic intensity (A/m x 10^{-3})

a. Layer 3 (Red Clay), Normal Polarity. Demagnetization of this sample is typical of the laminated red clay (Layers 3-5)

b. Layer 8 (Gray Silt), Sample L8B1, Mixed Polarity. This sample has a normal declination (with a pronounced westerly component), but a reversed inclination.

c. Layer 8 (Gray Silt), Sample L8C1, Mixed Polarity. This sample has a reversed declination with a normal inclination.

Figure 7. ^{10}Be – $^{26}Al/^{10}Be$ Diagram Showing Cosmogenic-Nuclide Measurements from Riverbluff Cave Sediment. This diagram is a graphical solution to the simultaneous equations 1 & 2 in the text. Note that axes are plotted on an arithmetic scale instead of the more-usual logarithmic. The superscripted stars on the axis labels indicate that the measured nuclide concentrations are normalized to the surface ^{10}Be and ^{26}Al production rates, calculated as described in Appendix I. For additional discussion of this type of diagram see Granger (2006). The contours of age and erosion rate reflect the ^{10}Be decay constant of Nishiizumi et al. (2007) and the subsurface nuclide production of muons according to Heisinger et al. (2002,a,b).

Appendix I

Cosmogenic-nuclide measurements

Quartz grains within the cave sediment are predominantly chert from local limestone bedrock and residuum. As the cave roof consists of the same bedrock, sparse chert nodules could have been deposited inside the cave by rockfall from the cave roof. However, these chert nodules are uniformly larger than a few cm in size and are easily distinguishable from fluvially transported chert grains. Thus, we extracted medium to coarse sand (0.125–0.85 mm) from cave sediment by disaggregating in water and wet-sieving, then isolated quartz grains by carbonate dissolution in HNO_3 or HCl, and repeated etching in dilute HF. Al concentrations in the resulting quartz separates were 100–150 ppm. We extracted Al and Be from quartz separates by standard methods of HF dissolution and column chromatography (Stone, 2004), determined total Al concentrations by ICP optical emission spectrophotometry on aliquots of the dissolved sample, and measured Al and Be isotope ratios by accelerator mass spectrometry at the Center for Accelerator Mass Spectrometry, Lawrence Livermore National Laboratory. Total carrier and process blanks varied between 5700 ± 2200 and 17300 ± 4200 atoms ^{10}Be and between 22000 ± 22000 and 65000 ± 50000 atoms ^{26}Al, and were always less than 0.1% of the total number of atoms measured. The Be isotope ratio measurements were originally normalized to the standard KNSTD3110 (Nishiizumi, 2002); however, we have renormalized them to the 07KNSTD3110 standard (Nishiizumi et al., 2007). Table 5 in the text and Table I-1 here show the resulting measured ^{26}Al and ^{10}Be concentrations. The Al isotope ratio measurements are normalized to the KNSTD standards (Nishiizumi, 2004).

Burial age calculations

Burial ages are calculated from Equations (1) and (2) in the text (repeated below) and as discussed in the text.

$$N_{10,m} = \frac{P_{10}(0)}{\lambda_{10} + \frac{\varepsilon}{\Lambda}} e^{-\lambda_{10} t_b} + \frac{P_{10}(z_b)}{\lambda_{10}} \left[1 - e^{-\lambda_{10} t_b}\right] \qquad \text{(I-1)}$$

$$N_{26,m} = \frac{P_{26}(0)}{\lambda_{26} + \frac{\varepsilon}{\Lambda}} e^{-\lambda_{26} t_b} + \frac{P_{26}(z_b)}{\lambda_{26}} \left[1 - e^{-\lambda_{126} t_b}\right] \qquad \text{(I-2)}$$

In solving Equations (1) and (2), we computed nuclide production rates due to muons using a MATLAB implementation, described in Balco et al. (2008) of the method of Heisinger et al. (2002a, 2002b). We computed nuclide production rates due to spallation using the scaling scheme of Stone (2000) and the production rate calibration data set described in Balco et al. (2008). The burial depth of our samples (7100 g cm^{-2}) reflects the measured thickness (26.5 m) and rock density (2.68 g cm^{-3}) of the cave roof overlying the sample site. We took the mean elevation of the Ward Branch watershed upstream of the cave to be 350 m (1150 ft). We used values of $5.10 \pm 0.26 \times 10^{-7}$ yr^{-1} and $9.83 \pm 0.25 \times 10^{-7}$ yr^{-1} for the ^{10}Be and ^{26}Al decay constants, respectively (Nishiizumi et al., 2007; Nishiizumi, 2004).

ERROR ANALYSIS

We used a 10,000-iteration Monte Carlo simulation to calculate the uncertainties in the burial ages. We report both internal and external uncertainties in Tables 5 (Text) and I-1 (below). The internal uncertainties include only measurement uncertainty in the nuclide concentrations. The external uncertainties also include uncertainties in the nuclide production rates by spallation (Balco et al., 2008) and muons (from uncertainties in the cross-section measurements in Heisinger et al. (2002a and 2002b), uncertainties in the ^{26}Al and ^{10}Be decay constants, and a 5% uncertainty in the burial depth. By far the most significant uncertainties are the measurement uncertainties in the nuclide concentrations and the uncertainties in the decay constants; the others are minor by comparison. Finally, we also incorporated the geological constraint that our samples are stratigraphically ordered into the uncertainty estimate, by rejecting the results of Monte Carlo iterations that did not yield ages in the correct stratigraphic order. This generally follows the approach of Muzikar and Granger (2006), except that we used a Monte Carlo simulation instead of their analytical solution. As the burial ages of adjacent samples overlap within their uncertainties in all cases, this step results in a small adjustment of the most likely values for the ages, as well as a small decrease in the formal uncertainty of the ages, relative to the ages computed without considering the stratigraphic relationship of the samples (Table I-1, Fig. I-1).

Figure Caption

Figure I-1. Probability diagram. Results of Monte Carlo estimate of the uncertainty in the burial ages. The gray histograms show uncertainty distributions for each burial age when each sample is considered individually. The black histograms show the uncertainty distributions when the stratigraphic relationship of the samples is taken into account. The dotted line shows the Brunhes-Matuyama paleomagnetic boundary. As this figure is intended to show the relationship between the individual ages, it reflects measurement uncertainty only. Errors in the decay constants would have the effect of shifting the entire array of ages together.

Additional References

Balco, G., Stone, J.O., Lifton, N.A., and Dunai, T.J., 2008, A complete and easily accessible means of calculating surface exposure ages or erosion rates from 10Be and 26Al measurements: Quaternary Geochronology, v. 2, p. 174–195.

Heisinger, B., Lal, D., Jull, A.J.T, Kubic, P. Ivy-Ochs, S., Neumaier, S., Knie, K.,Lazarev, V., and Nolte, E., 2002a, Production of selected cosmogenic radionuclides by muons: 1. Fast muons: Earth and Planetary Science Letters, v. 200, no. 3–4, p. 345–355.

Heisinger, B., Lal, D., Jull, A.J.T, Kubic, P. Ivy-Ochs, S., Knie, K.,Lazarev, V., and Nolte, E., 2002b, Production of selected cosmogenic radionuclides by muons: 2. Capture of negative muons. Earth and Planetary Science Letters, v. 200, no. 3–4, p. 357–369.

Muzikar, P. and Granger, D., 2006, Combining cosmogenic, stratigraphic, and paleomagnetic information using a Bayesian approach: General results and an application to Sterkfontein: Earth and Planetary Science Letters, v. 243, p. 400–408.

Nishiizumi, K., 2002, ^{10}Be, ^{26}Al, ^{36}Cl, and ^{41}Ca AMS standards: Abstract O16-1, *in* 9th Conference on Accelerator Mass Spectrometry, p. 130.

Nishiizumi, K., 20 04, Preparation of ^{26}Al AMS standards: Nuclear Instruments and Methods in Physics Research B, v. 223–224, p. 388–392.

Stone, J. O., 2000, Air pressure and cosmogenic isotope production: Journal of Geophysical Research, v. 105 (B10), p. 23753–23759.

Stone, J. 2004, Extraction of Al and Be from quartz for isotopic analysis. UW Cosmogenic Nuclide Lab Methods and Procedures. URL http://depts.washington.edu/cosmolab/chem.html

Table 1. Faunal List from "mammoth horizon" (Layers 6/7) in Riverbluff Cave.

Taxon	Elements
Mammuthus	1. Tibia (partial, adult). 2. Scapula (partial, adult). 3. M2 molar (juvenile). 4. Rib (partial, juvenile). 5. Jugal (juvenile).
Equus	1. Metacarpal (partial). 2. Tarsal.
Testudines (Turtle)	Shell fragments from two individuals.
Vulpes (fox)	One canine.
Serpentes (snake)	One vertebra.
Aves	Numerous leg bones.

Note: We thank Larry Agenbroad and Greg McDonald for examining the mammoth and horse bones, respectively, and confirming their identification.

Table 2. Sediment layers in Riverbluff Cave.

Sequence	Layer	%Sand	%Silt	%Clay	Comments
One (Red Clay)	1	0	41	59	Bioturbated, textural percentages exclude small (rodent) bones.
	2	0	59	41	Bioturbated, bone fragments excluded.
	3	2	58	40	Laminated, normal polarity.
	4	7	53	40	Laminated, normal polarity.
	5	13	47	40	Laminated, normal polarity.
Two (Gravel Beds)	6	49	20	31	Vertebrate fragments concentrated along boundary between 6 & 7.
	7	62	16	22	Layers 6 & 7 contain abundant
gravel					and larger clasts.
Three organics, (Gray Silt)	8	6	67	27	Laminated with abundant Reversed polarity.
Four (Coarse Sand & Gravel)	9	49	20	31	Layers 9 & 10 contain low percentages of gravel.
	10	54	33	13	

Note: Textural percentages are for the ≤ 2mm fraction.

Table 3. Summary of paleomagnetic measurements, Layers 3-5.

Layer	Inclination (°)	Declination (°)	κ^a	α_{95}^b (°)	n^c
3	+54	350	225.	3.8	6
4	+49	356	51.	8.0	6
5	+54	359	90.	6.0	6

Note: Inclinations and declinations are vector means of six samples, five demagnetized under A.C. treatment and one with thermal. Individual inclinations and declinations are taken at the optimum demagnetization level (10 mT for A.F. and 350°C for thermal) based on vector intensity plots and the reproducibility of measurements in multiple orientations. A principal components analysis (PCA) of the individual samples' demagnetization sequence gives virtually identical orientations.

[a] Fisher precision parameter.
[b] 95% Confidence limit about the mean orientation.
[C] Number of samples per set.

Table 4. Paleomagnetic results, Layer 8.

Sample	Inclination (°)	Declination (°)	Treatment	Comments
L8-1	+72	352	A.F.	Does not demagnetize under A.F. treatment.
L8-2	+63	243	A.F.	Does not demagnetize under A.F. treatment.
L8-3	+85	153	A.F.	Does not demagnetize under A.F. treatment.
L8-4	+63	347	A.F.	Does not demagnetize under A.F. treatment.
L8-5	+68	335	A.F.	Does not demagnetize under A.F. treatment.
L8-6	+38	288	Thermal	Orientations trending toward reversed when cube disintegrated at 400°.
2L8C1	-5	51	Thermal	PCA[a]
2L8C3	+47	328	Thermal	PCA
L8B1	-34	297	Thermal	PCA
L8B2	+10	271	Thermal	
L8C1	+38	196	Thermal	PCA
L8C2	+10	357	Thermal	

Note: Orientations for A.F. samples are taken at the 10 mT demagnetization step, although these orientations are essentially constant through each step. Orientations for the thermal samples are taken at the optimum demagnetization level (generally 350° C), see explanation in Table 3 and text.

[a]Samples denoted by "PCA" had significant principal components, generally spanning demagnetization steps between 100 and 500°C.

Table 5. [a]Burial ages and paleomagnetic constraints for Riverbluff Cave sediment.

Layer	Sample Name	^{10}Be (10^6 atoms g^{-1})	^{26}Al (10^6 atoms g^{-1})	Burial Age (Ma)	Surface Erosion Rate Before Burial (m Ma^{-1})	Magnetic Polarity
5	RC-L5-F	1.909 ± 0.036	7.69 ± 0.31	0.648 ± 0.061 (0.079)	0.963 ± 0.063 (0.11)	Normal
6–7	RC-LHH-A	1.490 ± 0.038	6.18 ± 0.16	0.735 ± 0.053 (0.073)	1.306 ± 0.084 (0.15)	M/B Datum (0.78 Ma)
8	RC-L8-A	0.865 ± 0.030	3.383 ± 0.084	0.899 ± 0.055 (0.072)	2.16 ± 0.17 (0.26)	Reversed
9	RC-L9	1.442 ± 0.022	5.35 ± 0.17	0.963 ± 0.049 (0.068)	1.187 ± 0.061 (0.13)	
10	RC-L10	1.684 ± 0.026	5.62 ± 0.17	1.078 ± 0.055 (0.073)	0.883 ± 0.046 (0.10)	

[a] All error limits are at the 1-σ level. The first error limit for ages and erosion rates is the "internal uncertainty" which only accounts for analytical uncertainty in the nuclide concentrations. The larger values in parentheses are the total or external uncertainties which also take account of the uncertainty in nuclide production rates and decay constants. See Appendix I for additional discussion. All ages from Table 5 are rounded to two decimal places throughout the text. The Matuyama/Brunhes datum is placed between layers 5 and 8, based on the paleomagnetic sequence in Tables 3 and 4.

Table I-1. [a]Cosmogenic nuclide data.

Layer	Sample Name	^{10}Be (10^6 atoms g^{-1})	^{26}Al (10^6 atoms g^{-1})	Burial Age Considered Individually (Ma)	Burial Age Stratigraphically Constrained (Ma)	Surface Erosion Rate Before Burial (m Ma^{-1})
5	RC-L5-F	1.909 ± 0.036	7.69 ± 0.31	0.689 ± 0.080 (0.094)	0.648 ± 0.061 (0.079)	0.963 ± 0.063 (0.11)
6–7	RC-LHH-A	1.490 ± 0.038	6.18 ± 0.16	0.711 ± 0.063 (0.078)	0.735 ± 0.053 (0.073)	1.306 ± 0.084 (0.15)
8	RC-L8-A	0.865 ± 0.030	3.383 ± 0.084	0.960 ± 0.078 (0.090)	0.899 ± 0.055 (0.072)	2.16 ± 0.17 (0.26)
9	RC-L9	1.442 ± 0.022	5.35 ± 0.17	0.928 ± 0.064 (0.081)	0.963 ± 0.049 (0.068)	1.187 ± 0.061 (0.13)
10	RC-L10	1.684 ± 0.026	5.62 ± 0.17	1.068 ± 0.059 (0.079)	1.078 ± 0.055 (0.073)	0.883 ± 0.046 (0.10)

[a]This table lists data in Table 5 (text), but also compares the "raw" burial age determined directly from the isotope ratios with the final ages determined from the Monte Carlo analysis described above. The first uncertainties are the internal uncertainties, based on measurement error. The larger values in parentheses are the external uncertainties which also take account of uncertainty in nuclide production rates and decay constants.


Springfield
Plateau
Riverbluff Cave
0
100 km


Ward Branch Paleoentrance
East Passage
Cox Road
Figure 5
Blast Entrance
James River Paleoentrance


5 2 '02

METRIC
MR-6
C-THRU
FLEXIBLE / NON-SKID
STEEL


METRIC
cm
C-THRU
FLEXIBLE / NON-SKID
MR-6
STAINLESS STEEL
INCHES

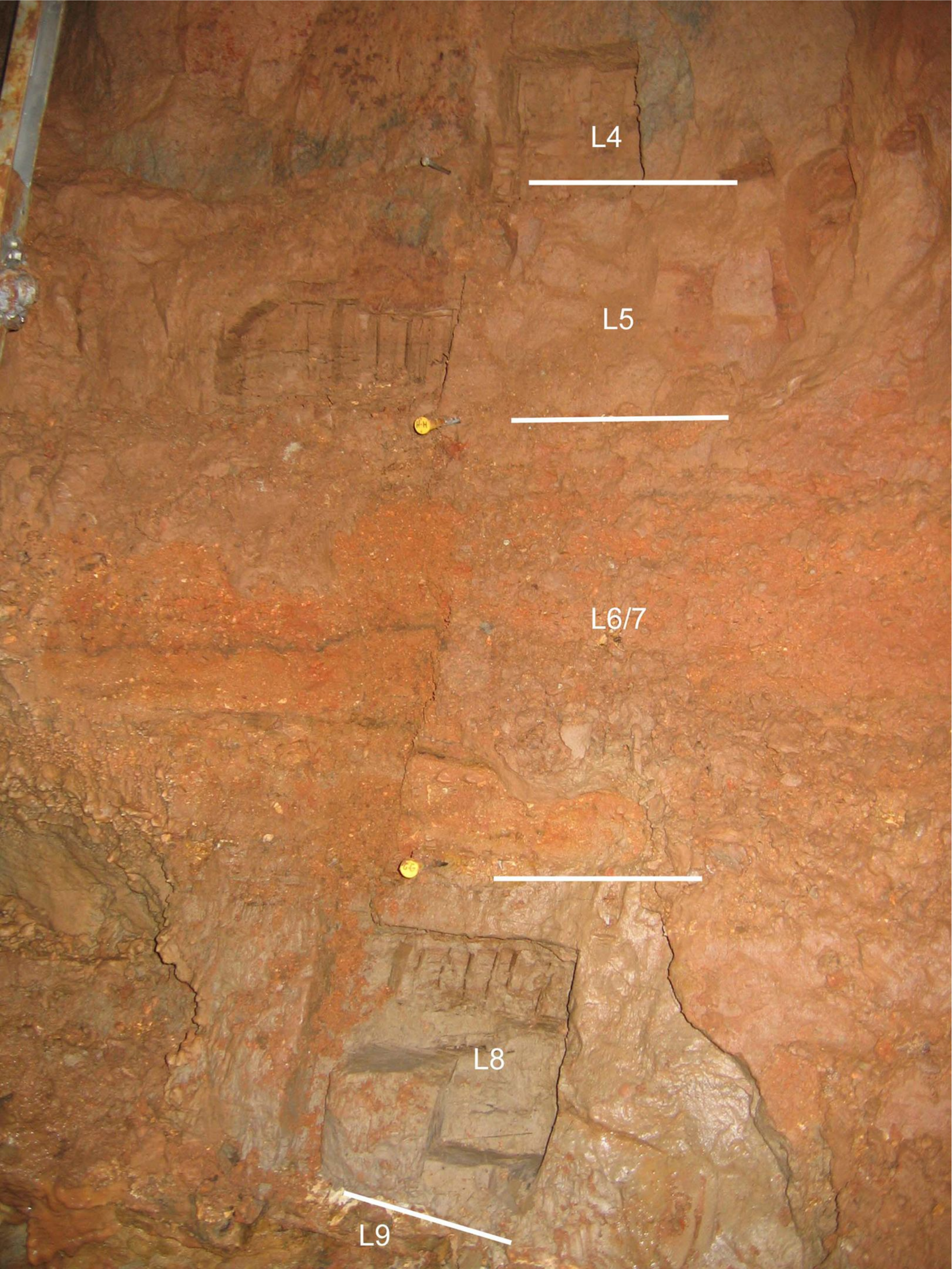
L4
L5
L6/7
L8
L9

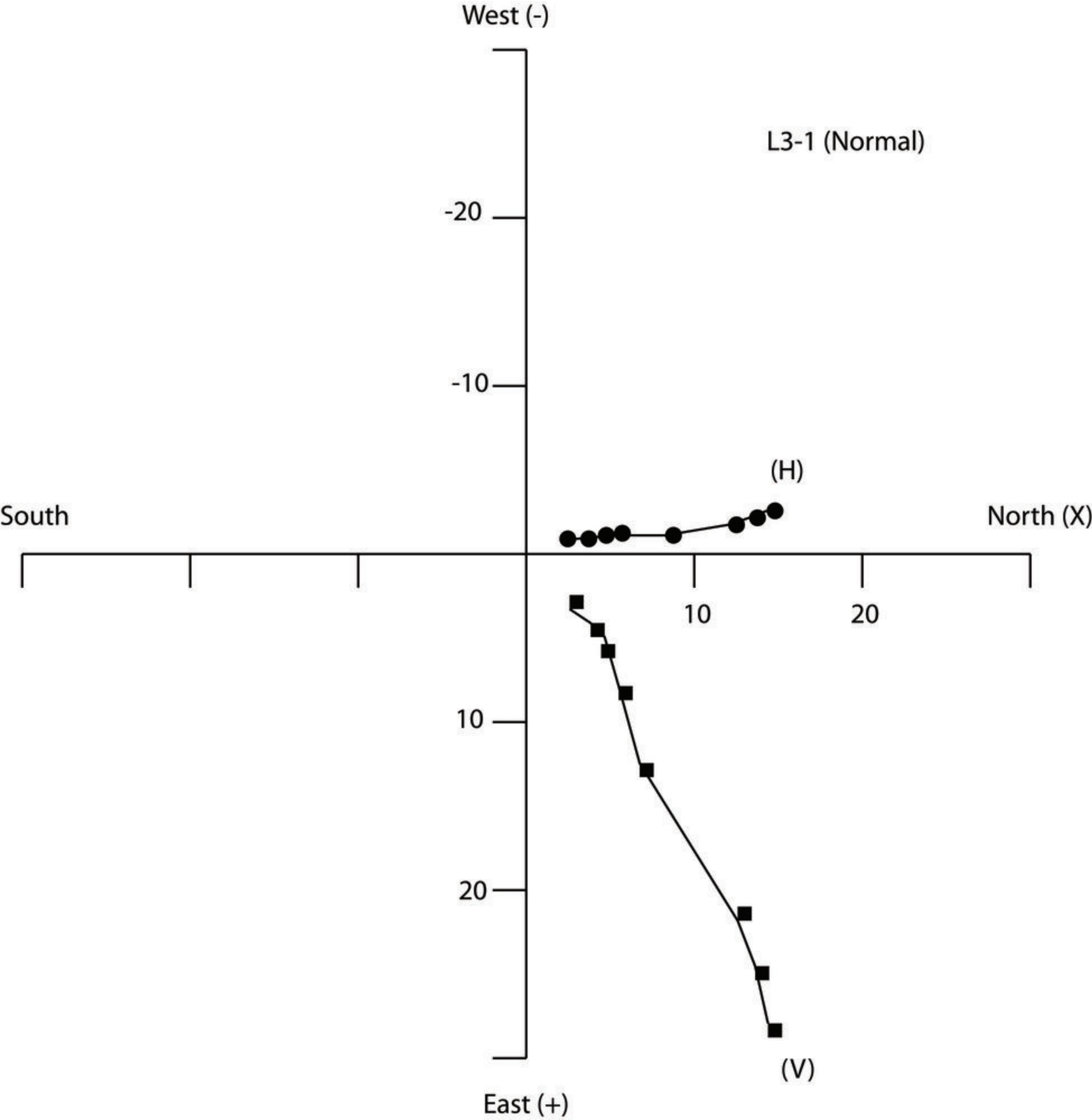
West (-)
L3-1 (Normal)
-20
-10
(H)
South
North (X)
10
20
10
20
(V)
East (+)

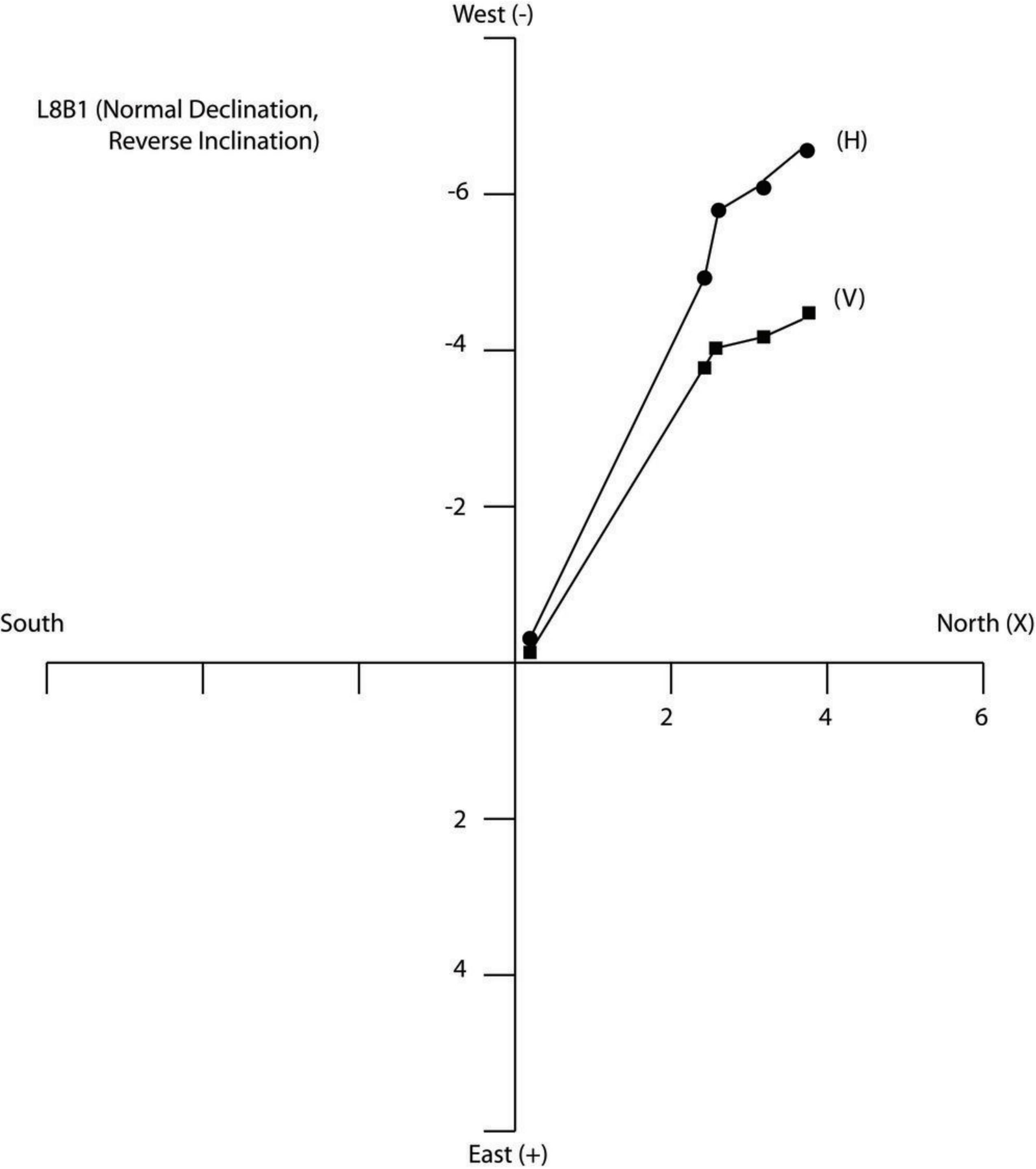
West (-)
L8B1 (Normal Declination,
Reverse Inclination)
(H)
(V)
-6
-4
-2
South
North (X)
2
4
6
2
4
East (+)

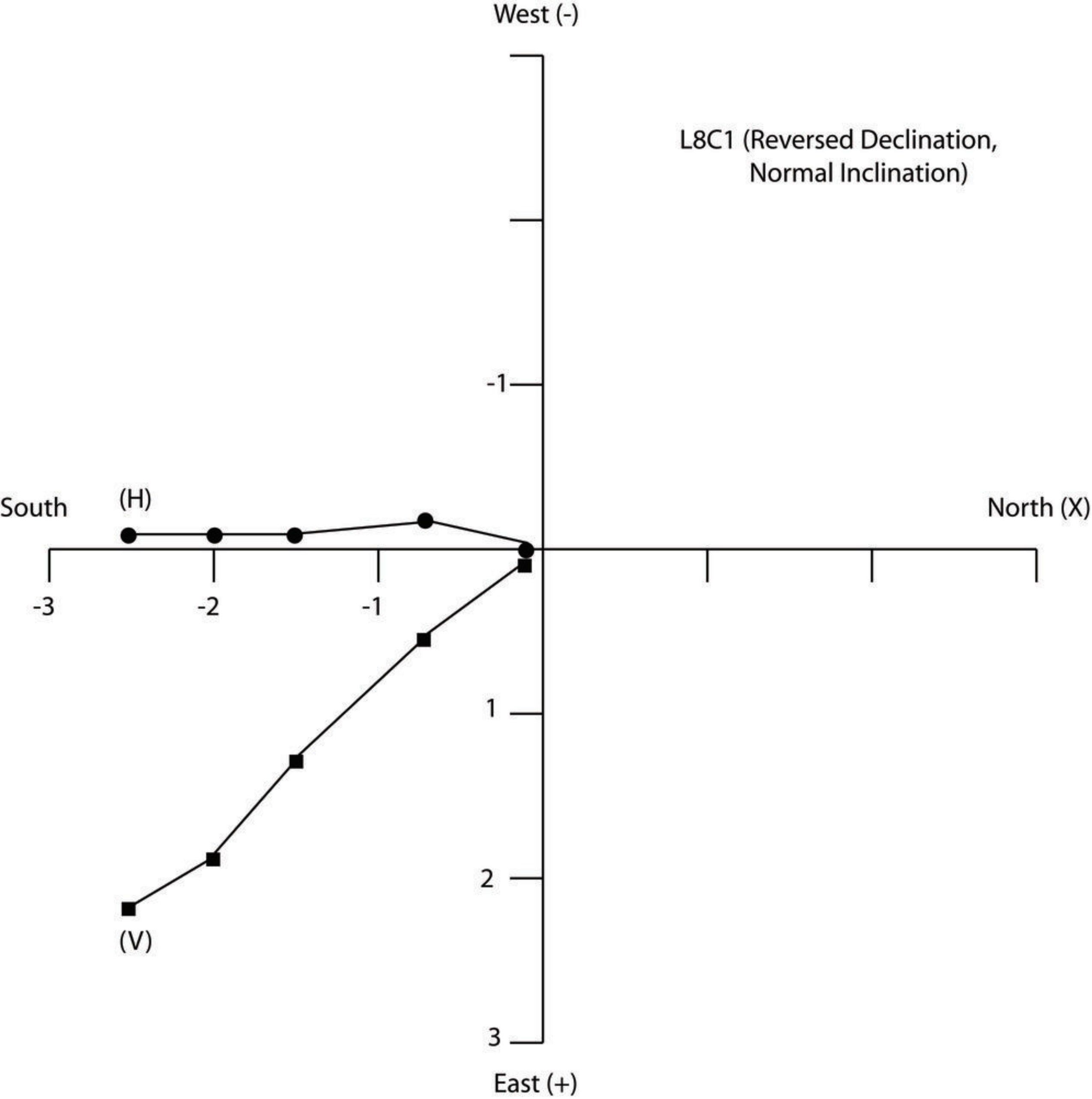
West (-)
L8C1 (Reversed Declination, Normal Inclination)
South
(H)
North (X)
-3
-2
-1
-1
1
2
3
(V)
East (+)

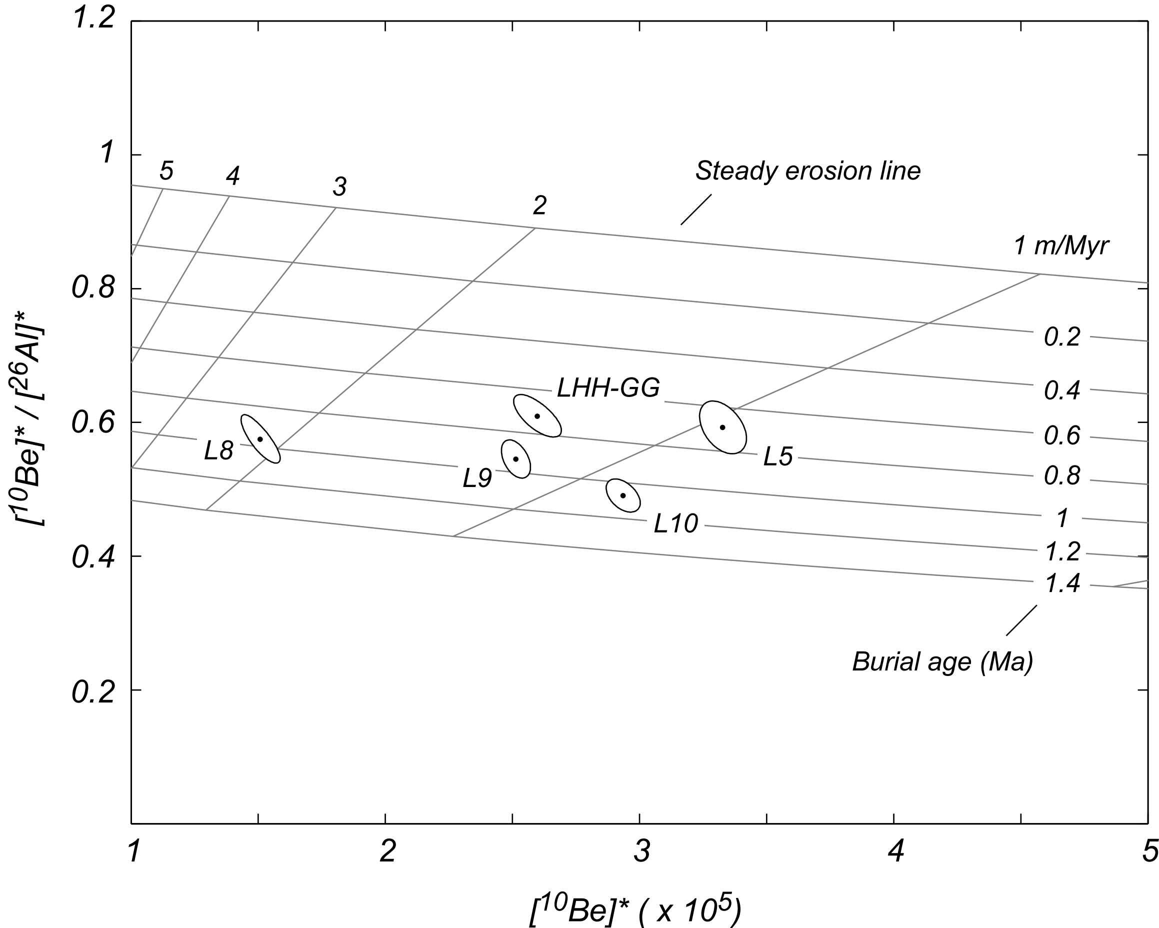

1.2
1
0.8
0.6
0.4
0.2
[10Be]* / [26Al]*
1
2
3
4
5
[10Be]* (x 105)
Steady erosion line
5
4
3
2
1 m/Myr
0.2
0.4
0.6
0.8
1
1.2
1.4
Burial age (Ma)
LHH-GG
L8
L9
L5
L10

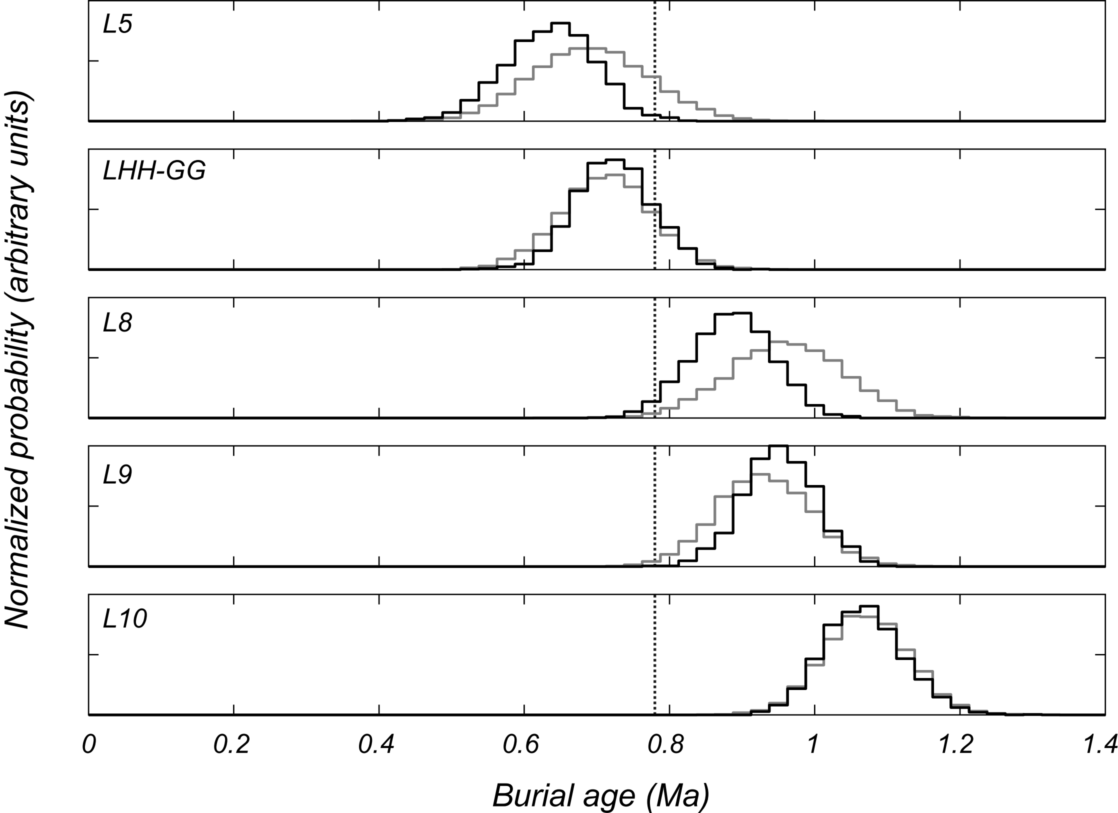
L5
LHH-GG
L8
L9
L10
Normalized probability (arbitrary units)
0
0.2
0.4
0.6
0.8
1
1.2
1.4
Burial age (Ma)